Using Radio Relics to Help Reconstruct the Dynamics of Galaxy Cluster Mergers

P.J. O'Mullan, D. Wittman
Physics Department, University of California Davis

Merging galaxy clusters are a unique environment in which to probe the behavior and properties of dark matter. Given that these events occur over billions of years, we cannot directly observe many of the parameters dictating the evolution of these events, and therefore must infer them through various methods. In the work of Wittman [11], these effects were inferred from extracting analog mergers from a large-scale n-body dark-matter cosmological simulation (BigMDPL). This method was largely successful in reproducing values consistent with observation for these inferred parameters. This work extends this method by predicting the shock location, which is not directly simulated by BigMDPL, for each analog merger. Comparison of these predicted locations with an observed shock location further narrows the set of simulated mergers that could match that observation.

I. INTRODUCTION

Constraining the properties of merging galaxy clusters is vital to determining their evolution over long periods of time. Understanding the evolution and dynamics of these massive events are crucial to gaining a deeper understanding of the various astrophysical events that occur within. Among those topics of study, one of the most fundamental is the behavior and properties of dark-matter.

Given the large timescale in which these events take place, many of the parameters needed to recreate the evolution of these events are not directly observable and must be inferred. Examples of such parameters include time since pericenter (TSP), velocity of the subclusters at pericenter, and whether the merger is in a returning or outbound phase. Various methods have been employed to study these systems and estimate their properties. Such methods include staged magneto-hydrodynamic simulations (MHD), n-body simulations, and Monte Carlo methods.

Previous work by Wittman [11] explored the use of a large scale cosmological n-body simulation known as BigMDPL, in which data concerning the simulated mergers was collected and stored for later comparison to real observations. When analyzing a real observation, the closest matching analogs from the recorded data were selected and used to estimate various non-observable parameters. This method promises a scalable, computationally inexpensive, and cosmologically motivated method to infer vital information about these systems.

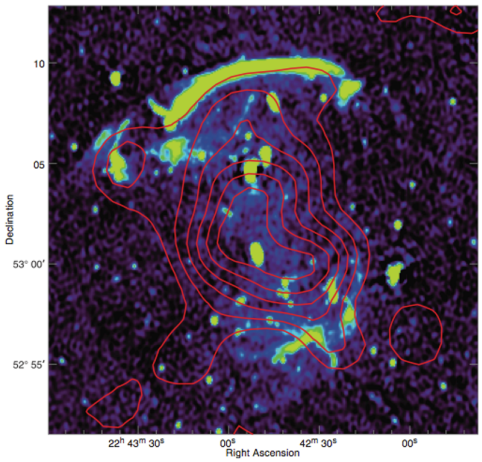

FIG. 1: X-Ray map of CIZA J2242.8+5301 with radio relics visible as the elongated green objects to the north and south of the image [10].

BigMDPL is a dark matter only simulation, meaning all particles in the n-body simulation are discrete chunks of dark-matter with no ordinary matter present. This simplification is used for large scale environments where investigation of the structure and formation of objects is key. Since dark-matter composes the majority of the mass in galaxy clusters, dark-matter only simulations are a good approximation of these systems.

This method provides a multitude of simulated analog "observations" with parameters that are motivated by the cosmological evolution of the simulated universe over time as well as contain large and small scale structure that may contribute in the evolution of the mergers and their parameters. This is in contrast to smaller scale staged simulations of specific cluster observations, with no cosmologically motivated parameters, nor large or small scale structure that may play a crucial role in the merger's evolution.

In merging galaxy clusters, ordinary matter emits radiation in the optical/near-infrared, radio, and x-ray regions [6]. These effects are useful in better understanding the properties of the system. The exclusion of ordinary matter from BigMDPL renders the simulation unable to model its role in these mergers and consequently must forego the corresponding observable astrophysical effects. This means that some observable quantities of a real system cannot be directly compared to their simulated counterparts. These effects would be accounted for in other types of simulations such as MHD and are part of the trade-off in choosing a cosmological n-body simulation.

This work explores the notion of extending Wittman's existing approach [11] to consider the location of radio relics in order to aid in resolving whether an observed system is in its outbound or returning phase (see Figure 2). Radio relics are regions of highly polarized diffuse synchrotron radio emission found in merging galaxy clusters. These regions (as seen in Figure 1) are suspected to be the result of a first order Fermi acceleration mechanism and their position is an indicator of the shock-front location [6]. The shock-front location is useful as it travels monotonically outward since first pericenter. The distance traveled by this shock-front can be used in conjunction with other estimated parameters already provided by the existing technique to better estimate of the system's phase.

One can see in Figure 2 that there is a symmetry in the observable locations of the galaxy subclusters during both the returning and outbound scenarios. This makes it difficult to tell at what point in the system's evolution we are observing the merger. In the second and fourth panels, the positions of the two subclusters are indistinguishable from one another, yet represent two different moments in the

evolution of this merger separated by possibly billions of years. We can resolve by noticing that the symmetry can be broken when considering the position of the radio relics.

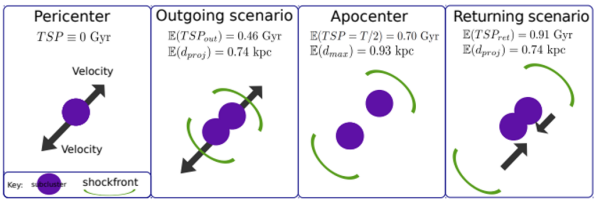

FIG. 2: Diagram of the various stages of a galaxy cluster merger. The symmetry of the subcluster positions are shown in the second and fourth panels, while the shock-front locations illustrate an observable distinction between the two panels [7].

To estimate the relic location, we use a similar model to that found in Ng et al. [7], where the location of a radio relic can be estimated using other parameters describing the system. This can then be used to compare the relic location of a real-world system, to the range of estimated relic positions of the many similar analogs in BigMDPL. This comparison will provide an indicator of the phase of the real-world system at the time of observation.

II. METHODOLOGY

Two modifications were made to the program in order to implement this analysis. Firstly, measurements of relic polarization were considered to narrow down the viewing angle. Secondly, we estimate the relic positions for each analog and build likelihood distributions stratified by returning and outbound analogs. We use these estimates to classify the real world observation based on where it falls relative to the pair of distributions.

A. Polarization & Viewing Angle

It has been shown that one can infer a bound on the viewing angle of an observable system by measuring the relic polarization fraction [4]. The polarization fraction is a byproduct of the shock-front emitted during a merger. The shock-front compresses and aligns unordered magnetic fields along the plane of the shock-front. Observation of the system with an viewing angle $\delta > 0$ with respect to the normal of the shock-front, results in the magnetic fields aligned by the shock-front and oriented in a preferential direction in the plane of the sky. Therefore, the radio signal received is polarized in that preferential direction. The polarization fraction is then the percentage of signal polarized in the preferential direction of the magnetic fields. For this analysis we assume a strong field and follow the arguments of Ensslin et al. [4]. Polarization in a strong field is given by,

$$\langle P_{strong} \rangle = \frac{\gamma + 1}{\gamma + \frac{7}{3}} \frac{\sin^2 \delta}{\frac{2}{15}\frac{13R-7}{R-1} - \sin^2 \delta}.$$

Here, δ is the viewing angle, γ is the spectral index of the electrons, and R is the compression ratio given in [3] as,

$$\gamma = 2\alpha + 1,$$

$$R = \frac{\alpha + 1}{\alpha - \frac{1}{2}},$$

where α is the radio spectral index. One can rearrange the equation for polarization to solve for viewing angle δ and obtain,

$$\delta = \sin^{-1}\left[\sqrt{\frac{\frac{2}{15}\frac{13R-7}{R-1}\langle P_{strong}\rangle}{1 + \frac{\gamma+\frac{7}{3}}{\gamma+1}\langle P_{strong}\rangle}}\right]. \quad (1)$$

This relation defines a curve describing the lowest possible viewing angle that could produce the observed measurement of polarization (Figure 3).

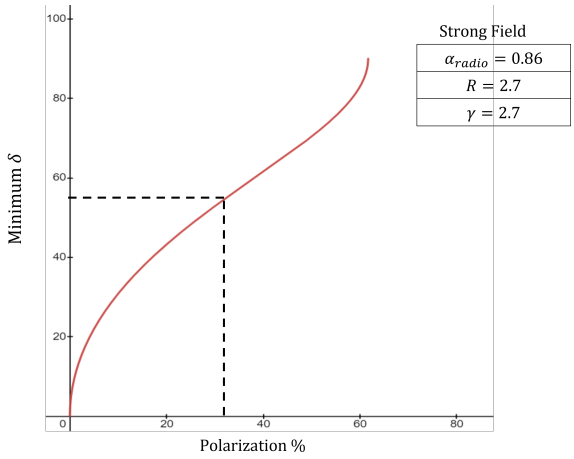

FIG. 3: Curve produced relating viewing angle to polarization measurement.

The program now considers the polarization measurements before it generates a mesh of viewing angles thereby generating more viewing angles within the likely range. This narrows down the range of relic locations as seen from a variety of angles.

B. Relic Location

For a simple case in which collisions are head on and relics remain on axis traveling along the separation vector of the two relics (i.e. a straight line can be drawn connecting both relics and both subclusters), we infer relic position with respect to the center of mass of the system using the following equation from [7],

$$s \approx \beta \frac{M_B v_{max}}{M_A + M_B} T_{SP} \sin \delta. \quad (2)$$

Where s is the distance from the relic to the center of mass, M_A and M_B are the masses of the more massive and less

massive subclusters respectively, T_{SP} is the time since pericenter, v_{max} is the maximum velocity of the two subclusters at pericenter, δ is the viewing angle, and β is an experimentally determined (unitless) constant controlling for errors in distance. The value of β usually ranges between 0.7 - 1.5. This generates a radius describing the expected distance of a relic from the center of mass of the system. This work did not study significantly off-axis systems. However, a mathematical model was developed to approximate such systems and is explained in the appendix. In the limit where the offset is zero, the off-axis model reduces down to the simpler on-axis model which will be used moving forward.

In this investigation, we do not consider the distance from a relic to the center of mass as a reliable metric. The primary reason for this decision is that the center of mass must be inferred via lensing analysis, which carries a high uncertainty. We instead chose to make use of more reliable observable quantities. Our primary metrics would be relic to relic distance and relic to nearest subcluster distance. These metrics are shown diagrammatically in Figure 4.

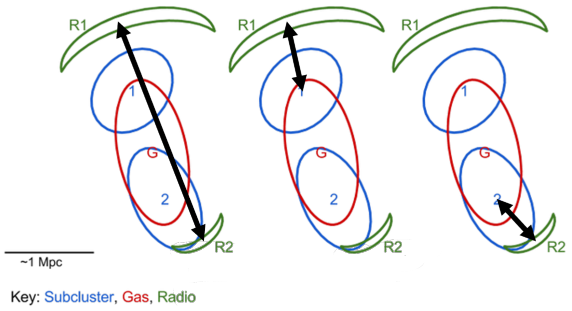

FIG. 4: Visual diagram of the metrics considered for comparison on an adapted diagram of CIZA J2242.8+5301 from the Merging Cluster Collaboration [5]. On the left one can see the relic to relic distance d_{r2r}, in the middle we have the distance between the first relic and its nearest subcluster d_{r1c1}, and on the right we have the distance between the second relic and its nearest subcluster d_{r2c2}.

The next step is to compute these estimations across the various analogs from the simulation and marginalize over viewing angles as well as values of β and build a distribution of analogs stratified by those outbound and returning.

The program starts by taking a single analog and extracting its parameters from the simulation (v_{max}, time since pericenter, etc.). It then explores how those parameters change under observation from a variety of viewing angles. Next, it computes a relic distance calculation across a range of different viewing angles and values of β. Each analog is classified as returning or outbound and the information is saved. The program then moves to the next analog until all have been processed.

The program then builds two histograms binned by distance and uses a kernel density estimator to approximate a distribution over that data. Real-world observations are plotted against these likelihood distributions and a metric to determine the phase of the merger is calculated by dividing the points of intersection for an observation and the two distributions (see Figure 5).

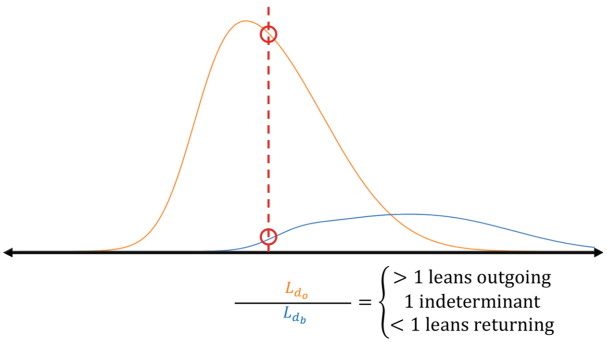

FIG. 5: An example of an observation (red dashed line) plotted against a returning (blue) and outgoing (orange) distribution. A metric is calculated by dividing the point of intersection with the outgoing distribution and observation by that of the returning distribution and observation.

III. RESULTS & DISCUSSION

This method was examined by using data from CIZA J2242.8+5301. The values used in the calculations were those found in Dawson et al. [1] and Stroe et al. [8] and can be found in Table **??**.

TABLE I: Table of values used in analysis. In this table α is the radio spectral index, **R** is the compression ratio caused from the shock front, γ is the spectral index of the electrons, d_{r2r} is the distance between relics, d_{rncn} is the distance between the north relic and it's nearest subcluster, and d_{rscs} is the distance between the south relic and its nearest subcluster.

Value	$\langle P_{strong} \rangle$	α	R	γ	d_{r2r}	d_{rncn}	d_{rscs}
	55%	0.77	6.56	2.54	2,600 kpc	850 kpc	450 kpc

During the program's run, it found and analyzed 1145 analog candidates from BigMDPL. It found a maximum viewing angle of $\delta \approx 64°$, which is consistent with the results found by Stroe et al. [9] where an angle within 30° of the plane of the sky was found. This translates to an angle greater than 60° for δ.

Our relic comparison metrics were also obtained and listed in the table below.

TABLE II: Table of results for our relic distance metrics. L_{rr} is the relic to relic metric, L_{rNcN} is the north relic to north cluster metric, L_{rScS} is the south relic to south cluster metric.

L_{rr}	L_{rNcN}	L_{rScS}
1.366	0.0047	8.467

From the table, our relic to relic metric leans very slightly towards an outgoing phase. The closeness in outgoing and returning phase likelihood is consistent with previous work supposing that CIZA J2242.8+5301 has at least passed first pericenter [2].

Our north relic to north cluster metric indicates an outbound scenario. It's higher likelihood as seen in Figure 6b makes also makes it a more reliable indicator.

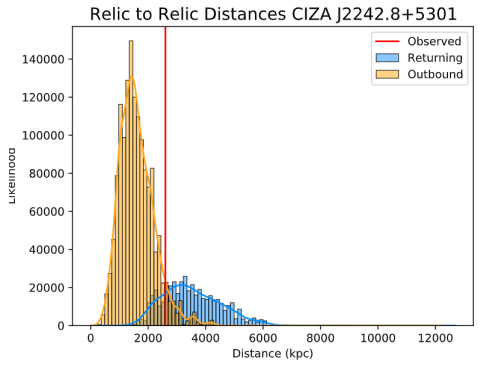

(a) Relic to Relic Distance for CIZA J2242.8+5301

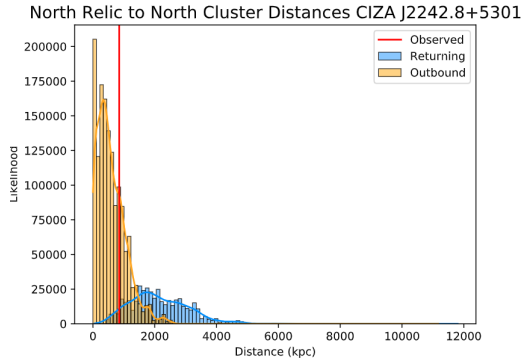

(b) North Relic to North Subcluster Distance for CIZA J2242.8+5301

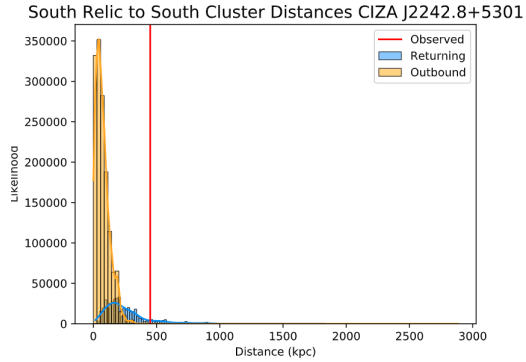

(c) South Relic to South Subcluster Distance for CIZA J2242.8+5301

FIG. 6: Distances for a run of the analysis tool on data for CIZA J2242.8+5301. The blue distribution represents the likelihood of analogs found at that distance for the returning scenario. The orange distribution represents the likelihood of analogs found at that distance for the outbound scenario. The red line represents the real world observed location of the radio relic for CIZA J2242.8+5301.

Our south relic to south cluster metric and figure yield the highest preference of all our metrics and favors a returning system. However, when looking at Figure 6c, one can notice the extremely low likelihood values at the corresponding distance location when compared to the majority of recorded analogs and the other metrics. Therefore, despite it's strong preference towards a returning phase, it's low relative likelihood makes it a less reliable indicator, although it should not be discounted entirely. It is possible that the BigMDPL simply did not contain enough appropriate analogs to obtain a more reliable result for this metric.

This information seems to indicate a slight preference for CIZA J2242.8+5301 to be an outbound merger overall. However, more data and further investigation is warranted to determine this with higher certainty.

IV. CONCLUSION

In this work we find that the analog method developed by Wittman [11] can be extended to estimate magneto-hydrodynamic parameters without the need for direct simulation. Our preliminary analysis of CIZA J2242.8+5301 is in good agreement with existing information and slightly favors CIZA J2242.8+5301 to be in its outbound phase following its first passage through pericenter.

Moving forward we plan to use this method to analyze the Bullet Cluster, another well studied cluster to further compare the results of yielded by this method to accepted data in literature generated by a variety of other methods.

The inconsistent reliability of our metrics for relic distances motivates further exploration CIZA J2242.8+5301 on larger cosmological simulations containing more potential analogs. Having more data also means that we are more likely to obtain more accurate estimates on our parameters.

In our analysis, we also noticed that the majority of analog candidates are in the outbound phase, regardless of which merger system we look at. This contributed to the lower overall likelihood of returning candidates. Further work needs to explore larger simulations to better understand if this is simply an artifact of our chosen simulation, or if there is something deeper to be explored. For more accurate estimations of relic distances, it may be worth investigating staged hydrodynamic simulations modeled from analogs found in dark-matter n-body cosmological simulations.

Appendix A: Consideration for Off Axis Relic

In this section we will go into detail to derive the mathematical model used to handle off-axis systems. We will start by deriving the equations approximating the location of the relics based on simple kinematics. Since the data recorded from the simulation considers the larger mass subcluster as an origin, we will need to change coordinates to the center of mass. We start by calculating the center of momentum (COM) frame of the system assuming that M_A is not moving and M_B is moving with velocity v_{max} towards M_A (so it has a negative sign).

$$\mathbf{V} = \frac{M_A v_A + M_B v_B}{M_A + M_B}$$

$$\mathbf{V} = -\frac{M_B v_{max}}{M_A + M_B} \tag{A1}$$

Now we can make a transformation from our inertial frame in M_A to the COM frame using the equation below.

$$v_{COM} = v - \mathbf{V} \tag{A2}$$

Using these equations and doing a bit of algebra gives the relative velocities of clusters A and B with respect to the center of mass. Which we then will multiply by β to control for error.

$$\langle v_A \rangle = \beta \frac{M_B v_{max}}{M_A + M_B} \tag{A3}$$

$$\langle v_B \rangle = -\beta \frac{M_A v_{max}}{M_A + M_B} \tag{A4}$$

From here it is easy to multiply these each by time since pericenter and obtain a range of their positions. One can note the similarity of this equation with those used in Ng et al. [7]. From here, we must consider three degrees of freedom that affect how we might observe a given analog if we viewed it as a real world observation. Those three parameters are the viewing angle δ, the angular offset between a relic and its nearest cluster ξ, and the orientation of the cluster in the sky ω. We can use these three values to estimate the distance between relics and their nearest clusters including off-axis systems. We can break this process down into a few steps.

1. Calculate the distance of the relics from the CM using the equations we derived above.
2. Generate two circles with each relic location at a point along the circle.
3. Input the observed angular offset between the line connecting the two mass clusters and the line connecting the two relics.
4. Parameterize the circles for the two relics and use that to derive the true angular offset between the relics and the clusters.
5. Generate a linear transformation matrix for rotations in $\mathbb{R}^3$ that projects a circle onto a plane (the sky) as an ellipse.
6. Reduce that transformation $\mathbb{R}^3 \rightarrow \mathbb{R}^2$.
7. Record the projected distance between the two relics and the distance between each relic and its nearest cluster.

Let us start by generating two circles of radius equal to our estimated relic distance and parameterize.

TABLE III: Information about the two relics. Listed in descending order, approximate distance from center of mass, circle mapping their radius, the parameterized equations for this circle

Relic A	Relic B
$s_A \approx \beta \frac{M_B v_{max}}{M_A + M_B} T_{SP}$	$s_B \approx -\beta \frac{M_A v_{max}}{M_A + M_B} T_{SP}$
$x_A^2 + y_A^2 = s_A^2$	$x_B^2 + y_B^2 = s_B^2$
$x_A = s_A cos(t)$	$x_B = s_B cos(t)$
$y_A = s_A sin(t)$	$y_B = s_B sin(t)$

Now that we have our circles, we now want to find the angular offset between our relics and our clusters. We do this so as to position the clusters horizontally along y=0 in this hypothetical coordinate space. Now that we have our circles, we now want to find the angular offset between our relics and our clusters. We do this so as to position the clusters horizontally along y=0 in this hypothetical coordinate space. This will require us to understand how this alignment changes with viewing angle. In order to do this, we will start with the equations for a parameterized ellipse.

$$x = \cos t,$$

$$y = k \sin t.$$

The variable k represents the ratio of the major and minor axis, and the variable t is our parameterized variable. We can further expand on this by allowing k, our ratio, to be a function of viewing angle.

$$k = \sin \delta$$

Now let us define points on opposite sides of this ellipse/circle where t is our initial angle.

$$x_1 = \cos t,$$

$$y_1 = k \sin t,$$

$$x_2 = \cos\left(t + \pi\right),$$

$$y_2 = k \sin\left(t + \pi\right).$$

Between these two points falls a line, a line which we can obtain the slope (note that b=0 since they are on opposite sides of the shape and will always cross zero).

$$y = mx + b,$$

$$m = \frac{y_2 - y_1}{x_2 - x_1}$$

$$\rightarrow m = \frac{k \sin(t + \pi) - k \sin t}{\cos(t + \pi) - \cos t}$$

After some algebra and substitution, we get a linear equation of the form,

$$y = (\sin \delta \tan t) x.$$

We can now obtain the angle that should be observed by us (Note, from here on out t will be referred to as ξ_{real} for

clarity). This gives us two equations, one to calculate the real angle from the observed, and vice versa.

$$\tan\xi_{obs} = \frac{y}{x} = \frac{(\sin\delta\tan\xi_{real})x}{x} = \sin\delta\tan\xi_{real}$$

$$\xi_{obs} = \tan^{-1}\left(\sin\delta\tan\xi_{real}\right) \tag{A5}$$

$$\xi_{real} = \tan^{-1}\left(\frac{\tan(\xi_{obs})}{\sin\delta}\right) \tag{A6}$$

From this we have our first transformation, it has a matrix of the form,

$$R_z(\xi_{real}) = \begin{bmatrix} \cos\xi_{real} & \sin\xi_{real} & 0 \\ -\sin\xi_{real} & \cos\xi_{real} & 0 \\ 0 & 0 & 1 \end{bmatrix}.$$

Now we consider the viewing angle transformation. For this we consider a rotation in the plane of the sky perpendicular to how our clusters are aligned at y=0.

$$R_y(\delta) = \begin{bmatrix} \cos\delta & 0 & \sin\delta \\ 0 & 1 & 0 \\ -\sin\delta & 0 & \cos\delta \end{bmatrix}.$$

These two transformations are sufficient to obtain our values, however for the sake of completeness, we could add another transformation about the z-axis, to account for alignment in the plane of the sky. I will denote this variable ω.

$$R_z(\omega) = \begin{bmatrix} \cos\omega & -\sin\omega & 0 \\ \sin\omega & \cos\omega & 0 \\ 0 & 0 & 1 \end{bmatrix}$$

From these three matrices, we can form a transformation matrix which I will refer to as $T_{\mathbb{R}^3}$.

$$T_{\mathbb{R}^3} = R_z(\omega)R_y(\delta)R_z(\xi_{real})$$

$$= \begin{bmatrix} \sin\delta\cos\omega\cos\xi_{real} + \sin\omega\sin\xi_{real} & \sin\delta\cos\omega\sin\xi_{real} - \sin\omega\cos\xi_{real} & \cos\omega\sin\delta \\ \sin\delta\sin\omega\cos\xi_{real} - \cos\omega\sin\xi_{real} & \sin\delta\sin\omega\sin\xi_{real} + \cos\omega\cos\xi_{real} & \sin\omega\sin\delta \\ -\sin\delta\cos\xi_{real} & -\sin\delta\sin\xi_{real} & \sin\delta \end{bmatrix}$$

We can now take this transformation down to $\mathbb{R}^2$ and denote the new transformation $T_{\mathbb{R}^2}$.

$$T_{\mathbb{R}^2} = \begin{bmatrix} \sin\delta\cos\omega\cos\xi_{real} + \sin\omega\sin\xi_{real} & \sin\delta\cos\omega\sin\xi_{real} - \sin\omega\cos\xi_{real} \\ \sin\delta\sin\omega\cos\xi_{real} - \cos\omega\sin\xi_{real} & \sin\delta\sin\omega\sin\xi_{real} + \cos\omega\cos\xi_{real} \end{bmatrix}$$

Now we can transform our circle from before into a projected ellipse.

$$\begin{bmatrix} x' \\ y' \end{bmatrix} = T_{\mathbb{R}^2}\begin{bmatrix} x \\ y \end{bmatrix}$$

Notice that in our coordinate system we initially started with the relic positions at y=0 and rotated such that the clusters took those positions, so we can drop the y-terms.

$$\rightarrow \begin{bmatrix} x' \\ y' \end{bmatrix} = \begin{bmatrix} x(\sin\delta\cos\omega\cos\xi_{real} + \sin\omega\sin\xi_{real}) \\ x(\sin\delta\sin\omega\cos\xi_{real} - \cos\omega\sin\xi_{real} \end{bmatrix}$$

This then becomes

$$\begin{bmatrix} x' \\ y' \end{bmatrix} = \begin{bmatrix} \beta\frac{M_B v_{max}}{M_A+M_B}T_{SP}(\sin\delta\cos\omega\cos\xi_{real} + \sin\omega\sin\xi_{real}) \\ \beta\frac{M_B v_{max}}{M_A+M_B}T_{SP}(\sin\delta\sin\omega\cos\xi_{real} - \cos\omega\sin\xi_{real} \end{bmatrix}.$$

Notice that in the limit where the cluster is on axis, and we neglect how the cluster is oriented, these become,

$$\begin{bmatrix} x' \\ y' \end{bmatrix} = \begin{bmatrix} \beta\frac{M_B v_{max}}{M_A+M_B}T_{SP}\sin\delta \\ 0 \end{bmatrix}. \tag{A7}$$

This is exactly the equation used in the paper when discussing on axis cases. From here, we simply need to calculate relic-cluster distance (seen in Figure 7) as we can trivially calculate relic relic distance by performing this transformation for both relics.

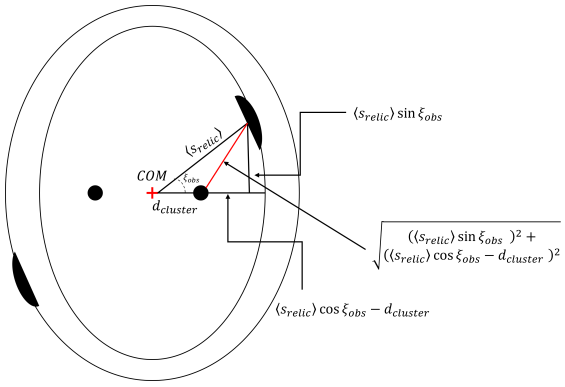

FIG. 7: Geometry behind getting relic-cluster distances.

Note that a disadvantage of this method is that we impose structure on each of the analogs by assuming the angular offset matches real-world observation instead of direct simulation.

Acknowledgements

This work was completed at the Research Experience for Undergraduates (REU) Program at The University of California Davis. Funded by NSF grant PHY-1852581

Bibliography

[1] Dawson, W. A., Jee, M. J., Stroe, A., Ng, Y. K., Golovich, N., Wittman, D., Sobral, D., Brüggen, M., Röttgering, H., and Van Weeren, R. (2015). Mc2: galaxy imaging and redshift analysis of the merging cluster ciza j2242. 8+ 5301. *The Astrophysical Journal*, 805(2):143.

[2] Dawson, W. A., Wittman, D., Jee, M. J., Gee, P., Hughes, J. P., Tyson, J. A., Schmidt, S., Thorman, P., Bradač, M., Miyazaki, S., Lemaux, B., Utsumi, Y., and Margoniner, V. E. (2012). DISCOVERY OF a DISSOCIATIVE GALAXY CLUSTER MERGER WITH LARGE PHYSICAL SEPARATION. *The Astrophysical Journal*, 747(2):L42.

[3] Drury, L. O. (1983). An introduction to the theory of diffusive shock acceleration of energetic particles in tenuous plasmas. *Reports on Progress in Physics*, 46(8):973.

[4] Ensslin, T. A., Biermann, P. L., Klein, U., and Kohle, S. (1997). Cluster radio relics as a tracer of shock waves of the large-scale structure formation. *arXiv preprint astro-ph/9712293*.

[5] MC2 (2014). Ciza j2242.8 5301.

[6] Molnar, S. M. (2016). Cluster physics with merging galaxy clusters. *Frontiers in Astronomy and Space Sciences*, 2:7.

[7] Ng, K. Y., Dawson, W. A., Wittman, D., Jee, M. J., Hughes, J. P., Menanteau, F., and Sifón, C. (2015). The return of the merging galaxy subclusters of el gordo? *Monthly Notices of the Royal Astronomical Society*, 453(2):1531–1549.

[8] Stroe, A., Harwood, J. J., Hardcastle, M. J., and Röttgering, H. J. A. (2014). Spectral age modelling of the 'Sausage' cluster radio relic. *Monthly Notices of the Royal Astronomical Society*, 445(2):1213–1222.

[9] Stroe, A., Van Weeren, R., Intema, H., Röttgering, H., Brüggen, M., and Hoeft, M. (2013). Discovery of spectral curvature in the shock downstream region: Ciza j2242. 8+ 5301. *Astronomy & Astrophysics*, 555:A110.

[10] Van Weeren, R. J., Röttgering, H. J., Brüggen, M., and Hoeft, M. (2010). Particle acceleration on megaparsec scales in a merging galaxy cluster. *Science*, 330(6002):347–349.

[11] Wittman, D. (2019). Dynamical properties of merging galaxy clusters from simulated analogs. *The Astrophysical Journal*, 881(2):121.